Murine model preclinical assessment of PEGylated block copolymer targeting cognition and oxidative stress insults of Alzheimer's disease

Sutapa Som Chaudhury
IIEST Shibpur: Indian Institute of Engineering Science and Technology
Mridula Nandi
IISER-K: Indian Institute of Science Education and Research Kolkata
Krishna Kumar
IICB: Indian Institute of Chemical Biology CSIR
Bhuban Ruidas
IIEST Shibpur: Indian Institute of Engineering Science and Technology
Tapas Kumar Sur
RG Kar Medical College and Hospital: RG Kar Medical College
Parash Prasad
IICB: Indian Institute of Chemical Biology CSIR
Saikat Chakrabarti
IICB: Indian Institute of Chemical Biology CSIR
Priyadarsi De
IISER-K: Indian Institute of Science Education and Research Kolkata
Jaya Sil
IIEST Shibpur: Indian Institute of Engineering Science and Technology
Chitrangada Das Mukhopadhyay (chitrangadam@chest.iiests.ac.in)
IIEST Shibpur: Indian Institute of Engineering Science and Technology https://orcid.org/0000-0002-7245-4736

Research Article

Keywords: Alzheimer's disease, Amyloid beta, Cognition impairment, Mitochondrial bioenergetics, In silico simulation

Posted Date: February 1st, 2022

DOI: https://doi.org/10.21203/rs.3.rs-1303843/v1

Abstract

Misfolded peptide amyloid beta ($A\beta_{42}$), neurofibrillary tangles of hyper-phosphorylated tau, oxidative damage to the brain, neuroinflammation are distinguished determinants of Alzheimer's disease (AD) responsible for disease progression. This multifaceted neurodegenerative disease is challenging to cure under a single treatment regime until the key disease-determinants are traced for their sequential occurrence in disease progression. In an early report, a novel side-chain tripeptide containing PEGylated block copolymer has been tested thoroughly *in vitro* and *in silico* for the early inhibition of $A\beta_{42}$-aggregation as well as degradation of preformed $A\beta_{42}$-fibril deposits. The present study demonstrates a preclinical assessment of the PEGylated block copolymer in colchicine-induced AD mimicking murine model. The colchicine induced Wistar rats receiving an intranasal delivery of the block copolymer at a daily dosage of 100 µg/kg and 200 µg/kg body weights respectively for 14 days manifested a notable attenuation of behavioral deficit pattern, oxidative stress, and neurotransmitters' deficiency as compared to the untreated ones. The current study also reports the ameliorative property of the PEGylated compound for progressive neuroinflammation and decreased mitochondrial bioenergetics in astrocytoma cell line viz. U87. A closer look into the drug mechanism of action of a compact three-dimensional PEGylated block copolymer confirmed its disintegrative interaction with $A\beta_{42}$ fibril via an *in silico* simulation. The results obtained herein this study signify the potential of the novel PEGylated block copolymer to ameliorate the cognitive decline and progressive oxidative insults in AD, and may envision a successful clinical phase trial.

1 Introduction

Alzheimer's disease (AD) is the most common form of dementia prevalent in an elderly population. AD is explained as a multidimensional pathophysiologic condition, which includes the amyloidosis, intra-neuronal deposit of hyper-phosphorylated tau-aggregates, and several changes in a mitochondrial cascade [1–3]. The latter is in focus, being relevant to the occurrence of neuroinflammation in the central nervous system (CNS) [4]. Though there is still debate on the neuroprotective or neurotoxic role of neuroinflammation at very initial stage of neurodegeneration, several studies, including some genetic data, proved the neuroinflammation-dependent AD progression and cerebral deposition of serum amyloid [5]. Even several reports eminently discussed the increased rate of β-amyloid deposition in inflammatory conditions driven by the activated astrocytes and microglia [6]. Interestingly, amyloid-beta ($A\beta_{42}$) exhibits an indirect role in neuroinflammation stimulating reactive oxygen species (ROS) besides its intervention in direct neuronal damage [7]. The constant ROS-mediated activation of NF$\kappa\beta$ signaling, along with a high degree of astrogliosis and pro-inflammatory cytokines, leads to systemic inflammation [8]. Eventually, this acute systemic inflammation is proven to be associated with the cognition decline in AD patients not only in postmortem reports but also in animal experiments [8, 9]. Surprisingly, the neuroinflammatory condition can speed up tau-hyperphosphorylation, another causative factor in AD pathogenesis [10]. Influencing the situation, the tau-aggregates released by the dead neurons activate the microglial cells [11]. This clears that the therapeutic measure against AD would not be feasible following

any one-dimensional way of amyloidosis, tauopathy or neuroinflammation rather the combination of these three [12]. Due to these intertwined elements of the etiology of AD, the potent drug candidates ranging from peptidomimetics to small molecules and peptide-based biopolymers targeting the inhibition of pathogenic Aβ_{42}-aggregation ultimately fail in the human clinical phase trials [13]. Also, to have a potential therapeutic measure against AD, the missing link between the amyloid cascade hypothesis and the mitochondrial cascade hypothesis is to be found out. The major bioenergetic decline in between the asymptomatic metabolically compensated brain-aging phase, and the symptomatic metabolically uncompensated brain-aging phase; as posited by the mitochondrial cascade hypothesis, may enlighten with a clue in this regard [3]. Although, irrespective of the sequential occurrence, both the hypotheses consider almost the same phenomena associated with AD viz. the increased oxidative stress, mitochondrial dysfunction, inflammation, neuronal apoptosis, and so on [3, 14]. Therefore, to have a holistic therapeutic approach is of great importance in the premise where symptomatic drugs against AD are the only option to date.

Also, one of the main challenges for a successful preclinical assessment of AD drugs is their delivery crossing the blood-brain barrier (BBB) [15, 16]. Here lies the importance of the transmucosal nasal pathway-based drug delivery, circumventing the BBB [17]. Being in the vicinity of the cerebrospinal fluid (CSF) and the direct nervous interface to the brain, the highly vascularized olfactory region offers direct access to drugs from nose to brain [18]. This intra-nasal pathway provides a non-invasive mode of drug delivery as well as the stability to the peptide-based drugs of AD from degradation by plasma-trypsin, chymotrypsin, and other plasmatic enzymes [19, 20]. This nose to brain delivery is also advantageous in terms of high adsorption of large molecules avoiding gastrointestinal degradation and first-pass effect in the liver [18, 20].

Another key factor for the preclinical evaluation of AD drug candidates is to choose the animal model judiciously. Besides the transgenic mice (e.g., TG2576 AD mice) models used extensively in the *in vivo* studies, different chemically induced murine models also set a standard for several decades [21]. Streptozotocin, scopolamine, colchicine are some of the examples to induce cognitive impairments mimicking the condition in AD [22]. The colchicine-induced AD rat model is a well-established animal model to monitor the behavioral impairments over AD progression as well as an improvement in cognition upon treatment with a test drug [23]. Colchicine-induced AD mimicking model shows resemblance to AD pathophysiology through the loss of cholinergic neurons and neurofibers, significant change in acetylcholine transferase, glutathione, and acetylcholine level [24, 25]. Moreover, colchicine-induced lipid peroxidation causes oxidative damage to the rat brain leading to impairment of learning and memory [24]. In addition, the proven increase in amyloid beta-load in colchicine-induced AD murine model is helpful in evaluating the Aβ_{42}-aggregation targeting drug candidates [26].

In a previous report, we have shown the efficacy of a tripeptide side-chain-based PEGylated block copolymer [27]. Here we report the preclinical murine model-based studies for testing the efficiency of the previously reported compound as a competent drug candidate for AD. The major objectives were to correlate the expected cognitive improvement in colchicine-induced AD rats with surmounting of other

pathophysiological phenomena of AD, including mitochondrial dysfunction and neuroinflammation. In addition to bridge the *in vitro* and *in vivo* assessments of the drug candidate with future clinical trials, this study provides an *in silico* illustration of the drug mechanism of action.

2 Results

2.1 FITC-tagging and presence of inhibitor (I) in rat brain

In a previous report, we evaluated a PEGylated block copolymer with side-chain tripeptide-'LVF' for its efficacy to inhibit the early aggregation of misfolded Aβ_{42} peptide and oligomers as well as its capability to degrade the preformed fibrils of Aβ_{42} in *in vitro* and *in silico* models [27]. In this current study, the block copolymer has been reconstructed with a tag, namely fluorescein isothiocyanate (FITC), to trace its presence in rat brain while studying the inhibitor as a potent drug candidate for AD *in vivo*. The successful tagging with the FITC was confirmed through ^{1}H NMR, UV-Visible spectroscopy, and fluorescence measurement (Supporting Information). Further, the penetration of the FITC functionalized PEGylated block copolymer (Inhibitor, I) inside the rat brain following an intranasal drug delivery was detected through fluorescence spectra, and upon quantification, it was found that 24 nmole, 35 nmole, 18.26 nmole, and 12.78 nmole of I were present at 1 h, 6 h, 12 h, and 24 h respectively after the administration of final dose (Supporting Information, Figure S5, S6). Moreover, the slow rate of fluorescence decline may relate to the persistent efficacy of I. Further, the choice of intranasal drug delivery was worthy in comparison to the intravenous route, as indicated by the insignificant presence of I in rat brain following an intravenous delivery of I (Figure S6c).

2.2 Selecting the therapeutic dose based on acute toxicity

Two effective therapeutic intranasal doses of I were chosen for rats, based on the acute toxicity study. The intranasal LD_{50} dose of 'I' was determined 73 µg mouse dose, equivalent to 3650 µg/kg body weight for a mouse. Based on the LD_{50} dose, the therapeutic safe doses for rats were selected to 10 µg/10 µl and 20 µg/10 µl for their each nostril (Supporting Information, Table S3 & Figure S7). For this reason, everyday each rat received either 20 µg or 40 µg I, which were nearly 100 µg/kg and 200 µg/kg body weight, respectively.

2.3 Amelioration of cognitive decline and oxidative stress markers in AD rat model

The effect of I on colchicine-induced impairment of learning and memory were assessed by different behavioral studies like open-field and closed-field activity, Y-Maze test, elevated plus maze test (EPM), Step-down latency passive avoidance test, and Morris water maze test.

Open-field activity scores were noted as counts/5 min on day zero before intracerebroventricular (ICV) injection and day 28 after the treatment. The score was decreased to 31.6 from 64.0, to 11.1 from 24.6, and to 5.5 from 13.6 for AD rats as compared to sham on ambulation, rearing, and grooming,

respectively. The treated group which received 0.2% (2 mg/ml) of I showed significant improvement by scoring 51.6 (** $p<0.01$), 18.5 (** $p<0.01$), and 10.3 (*** $p<0.001$) as compared to AD on 28 day after treatment in ambulation, rearing and grooming respectively (Figure 1a). Similarly, the gross behavioral activity of the rats was tested through a closed-field study. In this test, the AD group scored 144.6 with respect to the 241.1 of sham on 28 day of the study whereas, the 0.1% and 0.2% treated groups scored 189.5 (** $p<0.01$) and 206.6 (*** $p<0.001$) respectively (Figure 1b). Proving a decline in the learning process, the AD rats scored 14.6% (*** $p<0.001$) spontaneous alteration in the Y-Maze test compared to the 63.1% spontaneous alteration scoring sham group on the 28th day. Interestingly, the 0.1% and 0.2% treated groups scored 27.6% (** $p<0.01$) and 34.5% (*** $p<0.001$) alteration showing an improvement in willingness to explore new environment. On testing the memory acquisition on 20th day of colchicine administration through EPM, the colchicine-induced AD rats lost the learning ability significantly, and it took 75 s initial transfer latency (ITL) to enter the closed arm compared to the sham rats, which has taken 40.3 s. The 0.1% and 0.2% treated groups showed ITL of 60 s and 53.16 s, respectively. When retention of the memory was tested on the 21st and 28th day, AD rat has taken 80.5 s for 1st retention transfer latency (1st RTL), and 78.3 s (2nd RTL) with respect to 18.1 s and 15.1 s RTL of the sham rats, respectively. Compared to this, 0.1% and 0.2% treated rats possessed 31.8 s, 28.5 s, 28.3 s, and 24.5 s of 1st and 2nd RTL, respectively. All the EPM data showed a significant difference level with $p<0.001$ in paired t-test. The passive avoidance paradigm projected the changes in the learning and memory patterns of the rats throughout the experimental period. A probable reason for this may be the inability of the drug candidate to pass the BBB.

During the acquisition trial on the 19th day after ICV injection of colchicine, the sham group has taken 189.3 s of step-down latency (SDL), where they received an electric shock of 20 V on stepping down the platform. The next day this group took more time (226.6 s) of SDL, and finally, their SDL increased to 260.6 s on the 27th day. This signified the spontaneous response of the control group whereas, the AD rats did not show any memory response and stepped down from the platform with decreasing SDL (Figure 1e). Interestingly, the treated groups showed improvement in memory response by consistently taking a long time to step down from the platform with a significance level $p<0.001$. Lastly, in the Morris water maze test, the spatial navigation ability of the experimental animals was tested, and it was found that the colchicine-induced AD rats showed higher acquisition latency (AL) and retention latency (RL) time than the control group indicating the impaired learning and memory. Also, the improvement of the treated groups in finding the platform within the cut-off time of 3 min imposed the reversal of memory and learning capability as compared to the AD group (Figure 1f).

There are pieces of evidence that acetylcholine-containing neurons contribute significantly to cognitive decline as observed in AD [28]. Acetylcholinesterase (AchE) plays a pivotal role in the metabolism of acetylcholine which acts as a neurotransmitter. Colchicine being responsible for increasing AchE and thereby degenerating cholinergic neurons in AD mimicking experimental animals provides a platform to evaluate the potential AD drugs (Kumar et al., 2007). In this current report, the level of AchE in colchicine-induced rats was significantly high compared to the control group, which got lowered upon treatment

with I (Figure 2a). Even higher the dose of I lower was AchE level (31.8%, $p<0.001$), which was correlated with overall improvement in cognition.

There are reports showing evidence for the correlation between cognitive declines and decreasing oxidative stress markers [30]. Besides evaluating the cognitive functions of experimental animals herein, we have tested the oxidative stress markers viz. lipid peroxidation (LPO), reduced glutathione (GSH), superoxide dismutase (SOD), and catalase activity. Measuring lipid peroxidation marker is the best tool to measure cellular oxidative damage due to oxidative degradation of membrane lipid. In colchicine-induced AD rats, the lipid peroxidation increased by 120% ($p<0.001$) in the hippocampus compared to the sham group, which upon treatment with 0.1% and 0.2% I got reduced by 23% and 31.5% ($p<0.001$) (Figure 2b). Similar results were obtained on analyzing the tissue from the cortex (Figure 2b). The cellular antioxidant, namely glutathione in its reduced form (GSH), scavenges free radicals and protects proteins from oxidative damage [31]. Colchicine prompted oxidative stress in Wistar rats by lowering down 65% and 68% total GSH in cortex and hippocampus, respectively, compared to the control rats. Treatment with I improved both cortex and hippocampus's condition by increasing GSH level 57%, 88%, 49%, and 69% in 0.1% and 0.2% treated rats, respectively (Figure 2c). In addition, GSH, SOD maintains redox balance by channelizing the superoxide radicals into a continuous oxidation/reduction pool [32]. Herein the results implied that colchicine driven reduction (74% and 77% in cortex and hippocampus respectively) in SOD was increased by 84% and 120% in cortex and 94% and 136% in the hippocampus in 0.1% and 0.2% treated rats, respectively (Figure 2d). It has already been proven that catalase functions as the final checkpoint to cellular oxidative damages by converting H_2O_2 into H_2O and O_2 [33]. ICV injection of colchicine led to a depletion of catalase by 51% and 56% in cortex and hippocampal area of the brain, respectively, in Wistar rats compared to the control ones. Upon treatment with 0.1% and 0.2% I, these rats exhibited an increase in catalase enzyme both in cortex and hippocampus by 29%, 41%, 37%, and 52%, respectively (Figure 2e). These results indicated the capability of I to improve overall redox balance and oxidative damage induced in Wistar rats by colchicine which mimics the oxidative damage in AD pathology. Importantly, the I-treated control group did not any significant effect in the behavioral and oxidative marker changes, indicating the neutral property of a drug candidate.

2.4 The reversal in neurotransmitters level

Brief profiling of neurotransmitters, mainly dopamine (DA), norepinephrine (NE), and 5-hydroxytriptamine (5-HT) in treated and untreated AD rats, revealed a decrease in AchE, and a significant increase in DA, NE, and 5-HT level in AD versus treated rats was made feasible with the treatment with I. In previous reports, down-regulated dopaminergic neurotransmitters were linked with the pathophysiology of AD [34]. As similar to the previous reports, the dopamine expression was higher in the cortex than the hippocampus in sham rats (Figure 2f) [34]. On exposure to colchicine, the dopamine level in the cortex got decreased in AD mimicking rats (57%) as compared to the sham, which upon treatment with the 0.1% and 0.2% I has been improved by (53% and 70%, Figure 2f). Besides DA, NE level got subsided notably in the hippocampus of AD rats compared to the control ones (Figure 2g). A dose-dependent treatment with I exhibited a 66% and 102% increase in hippocampal-NE level in treated rats, respectively, with respect to

the AD ones (Figure 2g). Also, the reduction in 5-HT was modulated 36% and 61% after a dose-dependent treatment of AD rats with 0.1% and 0.2% I, respectively (Figure 2h). Here also, the I-treated control group did not any significant effect in altering the neurotransmitter levels itself. These quantitative progressions in neurotransmitters in the cortex and hippocampus of treated rats were correlated with the cognition improvements throughout the experiment.

2.5 Quantitative amelioration of Aβ_{42} load in brain tissues

Through immunohistochemical analyses and Congo red staining of the cortex (frontal) and hippocampal brain tissues, it was found that Aβ_{42} load in the brain, specifically in cortex and hippocampus, was decreased (Figure S8-S11). The decrease in relative fluorescence intensity in immunohistochemistry was 68%, 81%, 71%, and 87% in frontal and hippocampal brain tissues on treating with 0.1% and 0.2% I compared to the AD brain tissue. This signified the lowering of the Aβ_{42} load indirectly but precisely. Similarly, the Congo red staining of the 0.1% and 0.2% treated frontal and hippocampal rat brain sections showed a 63%, 74%, 63%, and 67% decrease in relative fluorescence intensity, respectively, compared to the AD brain sections.

Also, the brain tissue histochemistry complemented this finding qualitatively (Figure S12). Disorganization, loss, and shrinkage of pyramidal cells and increased vacuolations of the granular cells were prominent in colchicine-treated rat brains (Figure S12b, S12f). Whereas 0.1% and 0.2% treated rat cortex and hippocampal sections were observed with a restoration, preservation, and reduction in apoptosis of small pyramidal cells as well as reduced vacuolations of granular cells. The clumping of pyramidal cells was proof of damage repair (Figure S12d, S12g).

2.6 *In vitro* analyses of the inhibitor for mitochondrial response in oxidative stressors and neuroinflammation

Encouraged the results obtained *in vivo*, the *in vitro* analyses of cellular mitochondrial responses in oxidative stress conditions were appraised. The cellular oxidative damage and its reversal were also observed in astrocytoma U87 cells, which were in complete agreement with the *in vivo* data. An 81% reduction in ROS generation by I at 1:3 ratio was significant (*** $p<0.001$) as compared to the Aβ_{42}-treated cells (Figure 3a). Notably, the inhibitor lowered the ROS generation in a dose-dependent manner as compared to the Aβ_{42} peptide-treated U87 cells (Figure 3a). Also, when tested with the aid of fluorescence activated cell sorter (FACS), the inhibitor-treated cells showed a reduction in ROS generation compared to the Aβ_{42}-treated cells (Figure 3b). These results were in complete agreement with the changes in pro and anti-inflammatory markers, namely TNF-α, IL-6, TGF-β, and IL-10. The ROS generation-induced increase in pro-inflammatory marker TNF-α was significantly high ($P<0.001$) as compared to the control, which was reduced to 72% when treated with I at 1:1 ratio ($P<0.001$) (Figure 3c). Similarly, the increased level of IL-6 in Aβ_{42}-treated cells was dropped by 54% when treated with the inhibitor (Figure 3d). Interestingly, the Aβ_{42}-treated U87 cells were coping with the damage repair by increasing the anti-inflammatory markers, viz. TGF-β and IL-10 as compared to the control (Figure 3e, 3f). The treatment with

I even enhanced this damage control by increasing the TGF-β and IL-10 levels by 108% and 458%, respectively compared to the Aβ_{42}-treated U87 cells.

The successful monitoring on the levels of inflammatory markers intrigued the survey on mitochondrial membrane potential (MMP) and oxygen consumption rate (OCR) upon treatment with I. Mitochondrial injury and subsequent reduction in MMP was observed in the case of Aβ_{42}-treated U87 cells via the spectral emission shift of JC-1 dye from red to green (Figure 4). Further, an 18% cell population of the inhibitor-treated cells has shown a reversal of MMP compared to the Aβ_{42}-treated U87 cells (Figure 4c, 4d). Moreover, the treatment of Aβ_{42}-treated U87 cells with the inhibitor clearly reflected the improvement in maximal respiration, proton leak, and subsequent ATP production at a significant level in a dose-dependent manner (Figure 5c-5f).

2.7 *In silico* modeling of the block copolymer and an illustration to drug-mechanism of action

In connection with our previous study, a complete structural dynamics of the PEGylated block copolymer has been obtained in this current report [27]. Previously we reported the tendency of the block copolymer to bind with the Aβ_{42} fibril, oligomer, and monomer with a hydrophobic competitive inhibition of the 'KLVFFA' core of Aβ_{42}. Here a compact 3D structure of the whole block copolymer (with 113 moieties of PEG and 10 units of side-chain tripeptides) has been deciphered running a reasonably long 1.5 μs Molecular dynamics (MD) simulation (Figure S13). Post simulation, an energetically stable structure was acquired (Figure S13b). In terms of the radius of gyration, the compactness of the simulated block copolymer was high (Figure S13c). Moreover, in comparison to the pre-simulated structure, the volume, geometrical diameter, radius, and geometrical shape coefficient of the post-simulated one was relatively low, indicating a better spatial arrangement of all the moieties in the latter one (Table S4). The surface charge distribution was another parameter to judge the stability of a 3D structure. Here the surface charge distribution of the post-simulated block copolymer also proved its stability in this current form (Figure S13d).

To portray the binding interaction of the PEGylated compound with the fibril structure of Aβ_{42}, the compact PEGylated compound was placed randomly within interacting distances (<=5 Å) at various faces of the Aβ_{42} fibril structure (PDB ID: 5KK3). During each complex (fibril + molecule) MD simulation run for 100 ns, the structural disintegration of the participating unit chain assemblies (Chain A- Chain I and Chain J- Chain R) was observed, and a change in root mean square deviation (RMSD) and inter-unit distance was calculated (Figure 6, S14). The complete disintegration of 9 monomer units (chain A-I and chain J-R) was occurred only when PEGylated compounds were placed on the A and J chain face of the fibril. Thus, a probable mode of interaction of the PEGylated compound that could disintegrate the 9 monomer units (chain A-I and chain J-R) of fibril structure of Aβ_{42} peptide (PDB ID: 5KK3) was identified in this exercise. This disintegration of the 9 monomer units (chain A-I and chain J-R) of fibril structure of Aβ_{42} peptide was in complete agreement with the energy utilization by the system and the occurrence of

endothermic reaction taken place in isothermal calorimetric (ITC) experimentation in our previously published report [27].

3 Discussion

In this study, the PEGylated block copolymer reflected a holistic approach of AD therapeutics impeding cognition decline, oxidative neuronal damage, and improving neuroinflammation and mitochondrial bioenergetics. Importantly, the experimental murine model selected for this study rationally provided the actual disease condition of AD. Colchicine-induced AD mimicking model combined the learning and memory deficit in rats with oxidative stress and declination in neurotransmitters. It was evidenced that colchicine can induce oxidative stress and cause neuronal damage by altering GABA/glutamate ratio and thereby increasing NOS production in the brain [35]. Also, ICV injection of colchicine in rats brings down the irreversible cytoskeletal disruption imitating the neuronal and synaptic loss in neurodegeneration [36]. In fact, colchicine was found to cause severe damage in the brain's hippocampal area, resembling the pathogenicity in AD [37]. A 14 days long treatment with the PEGylated block copolymer has shown a dual action in confronting both these pathophysiologies profound in sporadic AD. In this study, the selected cognition monitoring markers, viz. the open field, closed-field test, Y-Maze, EPM, and Morris water maze tests altogether reflected a notable improvement in learning and memory in the block copolymer treated rats as compared to the colchicine induced AD rats. Even the treated rats showed a significant improvement in retention pattern for spatial navigation tasks in a dose-dependent manner as tested in the Morris water maze study. Earlier, Grundman and Delaney reported that the neuronal changes mediated by the free radicals are most likely one of the causes for the behavioral deficit in AD patients [38]. Herein this study, the central redox sink-markers, namely GSH, SOD, catalase, and the rate of lipid peroxidation, were assessed to evaluate the degree of CNS-oxidative damage. To our surprise, each of these oxidative stress markers was improved at a significant level ($p<0.001$). This reflected the therapeutic coverage of the PEGylated block copolymer. AD is diagnosed with a usual reduction in neurotransmitters, namely acetylcholine, and overexpression of the enzyme acetylcholinesterase, which hydrolyzes the acetylcholine. In this study, we found that the treatment with the block copolymer lowered the acetylcholinesterase enzyme activity. Besides, the others neurotransmitter related to emotion and cognition, viz. DA, NE, serotonin were improved at a commendable level. Not only colchicine-induced oxidative stress in CNS but also the synthetic Aβ_{42} induced ROS generation in astrocytoma cell line U87 and its impairment by the PEGylated compound was assessed in the current study. The advantage of using U87 astrocytoma cell line was that these cells mimic the oxidative insult taken place during the AD progression. Moreover, Aβ_{42} mediated discrepancy in mitochondrial respiration (OXPHOS) and mitochondrial membrane potential and their respective reversals following the treatment with PEGylated compound were evidenced here. Though there are debates over the protective role of pro-inflammatory cytokines, pieces of evidence also posited the chronic neuroinflammatory effects of astrogliosis and pro-inflammatory cytokines in turn. A balance restored between the pro and anti-inflammatory cytokines in astrocytoma cells preceding the treatment with the PEGylated compound showed a promising result in this regard. Importantly, the colchicine-induced increase in Aβ_{42} load in rat-brain cortex and hippocampus,

and subsequent decrease in Aβ_{42} aggregates upon treatment with the PEGylated compound was observed via the immunohistochemical studies. This piece of proof has evidenced the Aβ_{42} aggregation-inhibition property of the PEGylated inhibitor which is in complete agreement with the observed drug mechanism of action by the *in silico* studies. In our earlier report, the binding tendency of the 'LVF' side chains of PEGylated compound with the exposed chains of Aβ_{42} fibril was projected [27]. Now we were keen to obtain a 3D model of the compact PEGylated compound. This current study reports a complete disintegration of 9 monomer units (chain A-I and chain J-R) of duplex Aβ_{42} fibril (PDB ID: 5KK3) by a compact *in silico* modeled PEGylated compound. It is worth noting that the inhibitor itself did not show any significant effect on the locomotor behavior, oxidative changes, neurotransmitter levels, and other parameters of the experimental rats, and was equivalent to the sham group. Thus, the drug likeliness of I was proven through the experiments done in this report.

4 Conclusion

The current study with earlier reported PEGylated block copolymer with side-chain tripeptide 'LVF' evinced a successful preclinical assessment in a colchicine-induced murine model of AD. The nose to brain drug delivery technique adapted here ascertained a reliable drug delivery bypassing the BBB for comparatively larger molecules. Though the drug mechanism of action suggested the affirmation against inhibition of amyloid cascade, the comprehensive therapeutic capability of the block copolymer encourages unwinding the tangled common factorials of mitochondrial cascade hypothesis, amyloidosis, and tauopathy.

5 Experimental Procedures

5.1 Synthesis and characterization of fluorescein isothiocyanate (FITC) functionalized block copolymer PEG-*b*-P(LVF-HEMA)

The FITC functionalized block copolymer (I) was synthesized with the aid of a reversible addition-fragmentation chain transfer (RAFT) polymerization reaction. Further, the block copolymer has been characterized for the structure, spectroscopic measures, phase transition pH, and toxicity (Supporting Information).

5.2 Cell lines

Human neuroblastoma namely SHSY5Y and astrocytoma cell line viz. U87 were purchased from the National Centre for Cell Science (NCCS), Pune, India. The cells were retrieved according to the supplier's protocol. The cells were further cultured in Dulbecco's modified eagle's media (DMEM) containing 10% fetal bovine serum, 100 µg/ml streptomycin, 100 IU/ml penicillin, and keeping in an incubator at 37 ºC in 5% CO_2.

5.3 Experimental animals

Adult female Swiss albino mice and Wistar rats of both sexes were used for acute toxicity studies and pharmacological studies, respectively. In toxicity studies, nulliparous and non-pregnant female animals were only used due to their higher sensitivity to toxic effects than the males. All animals were procured from the CPCSEA registered vendor (M/s Chakraborty Enterprise, R/N: 1443/PO/b/11/CPCSEA) and were kept and maintained in CPCSEA registered institutional animal house (*R/N 959/c/06/CPSEA*) following NIH animal welfare guidelines [39, 40]. The details of animal maintenance have been stated in supporting information.

5.4 Acute toxicity study and selection of therapeutic dose

The acute intranasal toxicity and the sub-chronic level dosage regimen of the inhibitor were determined in nulliparous and non-pregnant 10 week aged female Swiss albino mice (5 groups, N=3) with bodyweight between 20-25 g (Supporting Information). Based on the acute toxicity study, the lethal dose (LD_{50}) of the inhibitor was calculated, and two effective therapeutic intranasal doses of 10 µg/10 µl and 20 µg/10 µl for each nostril were chosen for rats accordingly. Therefore, the therapeutic doses were 0.1% (1 mg/ml) and 0.2% (2 mg/ml), respectively. The test drug was prepared freshly for every pharmacological experiment solubilizing it in PBS at pH 5.5.

5.5 Induction of AD in Wistar rats and study design

Three months old male and female Wistar rats with an average bodyweight 170-180 g were acclimatized in laboratory condition and divided into five following groups containing six animals (three male and three female) in each group (Table 1). All animals except the sham group and control group (i.e., normal control and the 'I'-treated group) were induced to develop AD by ICV administration of a single dose colchicine (15 µg/5 µl solution of artificial cerebrospinal fluid, ACSF/site/rat) through the Stereotaxic apparatus (Harvard Apparatus, USA) following the well-established protocol to draw chemically induced AD animal model [35] (Supporting Information).

Table 1
Different groups of experimental animals

Group I	**Normal Control**	**Sham operated**	**No treatment**
Group II	Control (Test-drug, I-treated)	0.1% inhibitor without colchicine induction	Treatment with 'I' (day 14-28)
Group III	Untreated AD	Colchicine induced	No treatment
Group IV	AD + Treated	0.1% Inhibitor	Treatment (day 14-28)
Group V	AD + Treated	0.2% Inhibitor	Treatment (day 14-28)

The animals were maintained and left for the progression of AD for 2 weeks. The treated groups viz. Group IV and V have received test drugs, i.e., the inhibitor at the prefixed daily doses after 2 weeks of colchicine administration and continued for another 2 weeks. Group II was administered with the 0.1% I daily for 2 weeks without colchicine induction to find out whether the test drug has any effect of its own on experimental parameters including locomotor behaviors, oxidative stress, level of neurotransmitters, histopathology, and so on. Behavioral, cognitive, biochemical, neurochemical, histopathological, and immunohistochemical assessments were conducted in scheduled time (Supporting Information, Table S6).

5.6 Transmucosal nasal drug delivery and drug absorption in the brain

The transmucosal nasal drug delivery was chosen as the mode of drug administration due to the higher molecular weight of the test drug, 'I'. Also, the intravenous (IV) administration of I was assessed to compare the efficiency of transmucosal nasal route, and as a proof of intranasal delivery concept (Supporting Information). Further, the FITC-tagged inhibitor (I) was traced for its presence in rat brains after the transmucosal nasal delivery (Supporting Information).

5.7 Behavioral studies, biochemical assays, and brain neurotransmitters' profiling

The gross behavioral activities of the experimental animals were tested through open-field and closed-field studies (Supporting Information). The willingness of the experimental animals to explore a new environment was observed via Y-maze test and the acquisition and retention of memory was judged through elevated plus maze and step-down latency passive avoidance test (Supporting Information). Also the spatial navigation capability of the AD rats and the I-treated rats was compared with the aid of Morris water maze test (Supporting Information).

After completing the study, on day 29, succeeding the colchicine injection, all animals were sacrificed by cervical dislocation. Subsequently, the biochemical estimations of AchE, LPO, GSH, SOD, and catalase in protein from cerebral complex and hippocampus, respectively were determined spectrophotometrically (Bio-Rad iMark microplate reader) (Supporting Information). Also, the pivotal neurotransmitters viz. DA, NE, and 5-HT from brain homogenates of cerebral complex, and hippocampus were quantified using enzyme-linked immunosorbent assay (ELISA) kits (CK bio-14551, CK bio-15079 and CK bio-13330). The optical densities were measured at 45 nm using an ELISA plate reader (Bio-Rad). The sensitivity of DA, NE, and 5-HT was 2.36 ng/L, 2.24 pg/ml, and 0.23 ng/ml, respectively.

5.8 Histopathology, immunohistochemistry, and Congo red staining of brain sections

The brain tissue samples from the frontal and hippocampus were taken and studied for the histopathology, immunohistochemistry, and Congo red staining to detect amyloid load, following the

protocols described in supporting information.

5.9 Determination of reactive oxygen species (ROS) level and pro and anti-inflammatory cytokines in U87 cell line

The level of ROS was measured via a fluorimeter and a FACS with the aid of 2′,7′-Dichlorofluorescein diacetate (DCF-DA). Also, the quantitative assessment of pro and anti-inflammatory cytokines viz. TNF-α, TGF-β, IL-6, and IL-10 were done through ELISA using separate kits (RAB0476, RAB0460, RAB0306, and RAB0244 from Sigma Aldrich) and following manufacturer's protocol (Supporting Information).

5.10 Measurement of mitochondrial membrane potential and cellular mitochondrial bioenergetics

Mitochondrial membrane potentials of U87 cells were determined exploiting the red to green fluorescence shift in the emission of a cationic fluorescence dye, namely JC-1 (Invitrogen) upon the mitochondrial membrane damage (Supporting Information). Also, the cellular mitochondrial bioenergetics viz. mito-stress was analyzed by calculating the OCR in the U87 cell line via the Seahorse XFe24 extracellular flux analyzer (Seahorse Bioscience, USA) (Supporting Information).

5.11 In silico molecular dynamics simulation

MD simulations were run to study the structural dynamics of the PEGylated compound as well as to illustrate the potential impact of the interaction between Aβ_{42} fibril (PDB ID: 5KK3) and the simulated structure of the compound. The 113 unit stretch of PEG along with 10 unit side-chain tripeptide viz. 'LVF' was simulated using the smile formula (Supporting Information, Figure S15) to obtain the 3D structure of the compound. The structural stability and dynamics of this 3D structure were analyzed through 1.5 μs long MD simulation. Next, the simulated compact structure of the compound was placed randomly within an interacting distance of 5 Å at various faces of Aβ_{42} fibril and for each complex (fibril + molecule) a 100 ns MD simulation run was performed. Fibril structure without the molecule was also run for MD simulation as a reference.

5.12 Statistical analyses

All the data were represented as mean ± SD of six rats in each group. For the *in vitro* experiments, data were represented as mean ± SD of three experimental sets. Statistical significant differences were calculated by ANOVA (paired t-test) where 'a' represents Sham vs. AD, 'b' represents AD vs. treated group; significance levels were denoted by * $p<0.05$, ** $p<0.01$, *** $p<0.001$.

Declarations

Acknowledgment

The authors acknowledge Dr. Sib Sankar Roy, Senior Principal Scientist, and HOD, Cell Biology and Physiology Department, for the execution of Seahorse experiment and fluorescence microscopic imaging studies.

Author contributions

SSC conceptualized the study and interpreted the results, and JS and CDM supervised it. SSC and TKS designed and performed most of the experiments with the help of KK, MN, BR, and PP. SC conceptualized and contributed to the design of *in silico* studies. KK performed the *in silico* studies. MN and PD contributed in the synthesis of FITC-tagged inhibitor. MN performed the synthesis of the inhibitor. PP performed the seahorse experiment and contributed in the fluorescence imaging studies. JS reviewed the *in silico* experiments and helped analyzing the respective data. BR reviewed the content and analyzed the seahorse experiment and imaging data. SSC analyzed all the data, composed the figures and wrote the manuscript. CDM secured the collaborations and execution of the work. All the authors minutely reviewed the content and approved the final version.

Statements and declarations

Funding

The authors did not receive support from any organization for the submitted work.

Declaration of interest

The authors have no competing interests to declare that are relevant to the content of this article.

Ethics approval

All animal experiments were approved (Reference: RKC/IAEC/17/03) by the committee for the purpose of control and supervision of experiments on animals (CPCSEA), R.G Kar Medical College and Hospital, Kolkata; West Bengal, India. The animals were maintained and treated according to the NIH animal welfare guidelines.

Data availability statement

The datasets generated during and/or analysed during the current study are available from the corresponding author on reasonable request.

Consent to participate and/or consent for publication

Not applicable

References

1. Hardy JA, Higgins GA (1992) Alzheimer's disease: the amyloid cascade hypothesis. Science 256:184–185. https://doi.org/10.1126/science.1566067
2. Maccioni RB, Farías G, Morales I, Navarrete L (2010) The revitalized tau hypothesis on Alzheimer's disease. Arch Med Res 41:226–231. https://doi.org/10.1016/j.arcmed.2010.03.007
3. Swerdlow RH, Burns JM, Khan SM (2014) The Alzheimer's disease mitochondrial cascade hypothesis: progress and perspectives. Biochim Biophys Acta 1842:1219–1231. https://doi.org/10.1016/j.bbadis.2013.09.010
4. Calsolaro V, Edison P (2016) Neuroinflammation in Alzheimer's disease: Current evidence and future directions. Alzheimer's Dement 12:719–732. https://doi.org/https://doi.org/10.1016/j.jalz.2016.02.010
5. Karch CM, Goate AM (2015) Alzheimer's disease risk genes and mechanisms of disease pathogenesis. Biol Psychiatry 77:43–51. https://doi.org/10.1016/j.biopsych.2014.05.006
6. Mandrekar-Colucci S, Landreth GE (2010) Microglia and Inflammation in Alzheimer's Disease, vol 9. CNS Neurol Disord - Drug Targets- CNS Neurol Disord
7. Akiyama H, Barger S, Barnum S et al (2000) Inflammation and Alzheimer's disease. Neurobiol Aging 21:383–421. https://doi.org/10.1016/s0197-4580(00)00124-x
8. Holmes C, Cunningham C, Zotova E et al (2009) Systemic inflammation and disease progression in Alzheimer disease. Neurology 73:768–774. https://doi.org/10.1212/WNL.0b013e3181b6bb95
9. Liu R-X, Huang C, Bennett DA et al (2016) The characteristics of astrocyte on Aβ clearance altered in Alzheimer's disease were reversed by anti-inflammatory agent (+)-2-(1-hydroxyl-4-oxocyclohexyl) ethyl caffeate. Am J Transl Res 8:4082–4094
10. Lyman M, Lloyd DG, Ji X et al (2014) Neuroinflammation: the role and consequences. Neurosci Res 79:1–12. https://doi.org/10.1016/j.neures.2013.10.004
11. Perea JR, Llorens-Martín M, Ávila J, Bolós M (2018) The Role of Microglia in the Spread of Tau: Relevance for Tauopathies. Front Cell Neurosci 12:172. https://doi.org/10.3389/fncel.2018.00172
12. Bronzuoli MR, Iacomino A, Steardo L, Scuderi C (2016) Targeting neuroinflammation in Alzheimer's disease. J Inflamm Res 9:199–208. https://doi.org/10.2147/JIR.S86958
13. Yiannopoulou KG, Anastasiou AI, Zachariou V, Pelidou S-H (2019) Reasons for Failed Trials of Disease-Modifying Treatments for Alzheimer Disease and Their Contribution in Recent Research. Biomedicines 7. https://doi.org/10.3390/biomedicines7040097
14. Agrawal I, Jha S (2020) Mitochondrial Dysfunction and Alzheimer's Disease: Role of Microglia. Front Aging Neurosci 12:252. https://doi.org/10.3389/fnagi.2020.00252
15. Banks WA (2008) Developing drugs that can cross the blood-brain barrier: applications to Alzheimer's disease. BMC Neurosci 9:S2. https://doi.org/10.1186/1471-2202-9-S3-S2
16. Som Chaudhury S, Das Mukhopadhyay C (2018) Functional amyloids: interrelationship with other amyloids and therapeutic assessment to treat neurodegenerative diseases. Int J Neurosci 128:449–463. https://doi.org/10.1080/00207454.2017.1398153

17. Djupesland PG, Messina JC, Mahmoud RA (2014) The nasal approach to delivering treatment for brain diseases: an anatomic, physiologic, and delivery technology overview. Ther Deliv 5:709–733. https://doi.org/10.4155/tde.14.41
18. Crowe TP, Greenlee MHW, Kanthasamy AG, Hsu WH (2018) Mechanism of intranasal drug delivery directly to the brain. Life Sci 195:44–52. https://doi.org/10.1016/j.lfs.2017.12.025
19. Fan Y, Chen M, Zhang J et al (2018) Updated Progress of Nanocarrier-Based Intranasal Drug Delivery Systems for Treatment of Brain Diseases. Crit Rev Ther Drug Carrier Syst 35:433–467. https://doi.org/10.1615/CritRevTherDrugCarrierSyst.2018024697
20. Som Chaudhury S, Sinha K, Das Mukhopadhyay C (2021) Intranasal route: The green corridor for Alzheimer's disease therapeutics. J Drug Deliv Sci Technol 102791. https://doi.org/https://doi.org/10.1016/j.jddst.2021.102791
21. Wisniewski T, Sigurdsson EM (2010) Murine models of Alzheimer's disease and their use in developing immunotherapies. Biochim Biophys Acta - Mol Basis Dis 1802:847–859. https://doi.org/https://doi.org/10.1016/j.bbadis.2010.05.004
22. Mahdi O, Baharuldin MTH, Nor NHM et al (2019) Chemicals used for the induction of Alzheimer's disease-like cognitive dysfunctions in rodents. Biomed Res Ther 6:3460–3484. https://doi.org/10.15419/bmrat.v6i11.575
23. Mohamed AR, Soliman GY, Ismail CA, Mannaa HF (2015) Neuroprotective role of vitamin D3 in colchicine-induced Alzheimer's disease in rats. Alexandria J Med 51:127–136. https://doi.org/10.1016/j.ajme.2014.05.005
24. Nakagawa Y, Nakamura S, Kaśe Y et al (1987) Colchicine lesions in the rat hippocampus mimic the alterations of several markers in Alzheimer's disease. Brain Res 408:57–64. https://doi.org/https://doi.org/10.1016/0006-8993(87)90358-1
25. Kumar A, Naidu PS, Seghal N, Padi SSV (2007) Neuroprotective Effects of Resveratrol against Intracerebroventricular Colchicine-Induced Cognitive Impairment and Oxidative Stress in Rats. Pharmacology 79:17–26. https://doi.org/10.1159/000097511
26. Joy T, Rao MS, Madhyastha S, Pai K (2019) Effect of N-Acetyl Cysteine on Intracerebroventricular Colchicine Induced Cognitive Deficits, Beta Amyloid Pathology, and Glial Cells. Neurosci J 2019:7547382. https://doi.org/10.1155/2019/7547382
27. Som Chaudhury S, Sannigrahi A, Nandi M et al (2019) A Novel PEGylated Block Copolymer in New Age Therapeutics for Alzheimer's Disease. Mol Neurobiol 56:6551–6565. https://doi.org/10.1007/s12035-019-1542-1
28. Terry AVJ, Buccafusco JJ (2003) The cholinergic hypothesis of age and Alzheimer's disease-related cognitive deficits: recent challenges and their implications for novel drug development. J Pharmacol Exp Ther 306:821–827. https://doi.org/10.1124/jpet.102.041616
29. Kumar A, Seghal N, Naidu PS et al (2007) Colchicines-induced neurotoxicity as an animal model of sporadic dementia of Alzheimer's type. Pharmacol Rep 59:274–283

30. Liu R-X, Huang C, Bennett DA et al (2016) The characteristics of astrocyte on Aβ clearance altered in Alzheimer's disease were reversed by anti-inflammatory agent (+)-2-(1-hydroxyl-4-oxocyclohexyl) ethyl caffeate. Am J Transl Res 8:4082–4094
31. Bajic VP, Van Neste C, Obradovic M et al (2019) Glutathione "Redox Homeostasis" and Its Relation to Cardiovascular Disease. Oxid Med Cell Longev 2019:5028181. https://doi.org/10.1155/2019/5028181
32. Polle A (2001) Dissecting the superoxide dismutase-ascorbate-glutathione-pathway in chloroplasts by metabolic modeling. Computer simulations as a step towards flux analysis. Plant Physiol 126:445–462. https://doi.org/10.1104/pp.126.1.445
33. Nandi A, Yan L-J, Jana CK, Das N (2019) Role of Catalase in Oxidative Stress- and Age-Associated Degenerative Diseases. Oxid Med Cell Longev 2019:9613090. https://doi.org/10.1155/2019/9613090
34. Nobili A, Latagliata EC, Viscomi MT et al (2017) Dopamine neuronal loss contributes to memory and reward dysfunction in a model of Alzheimer's disease. Nat Commun 8:14727. https://doi.org/10.1038/ncomms14727
35. Veerendra Kumar MH, Gupta YK (2002) Intracerebroventricular administration of colchicine produces cognitive impairment associated with oxidative stress in rats. Pharmacol Biochem Behav 73:565–571. https://doi.org/10.1016/s0091-3057(02)00838-9
36. Emerich DF, Walsh TJ (1990) Cholinergic cell loss and cognitive impairments following intraventricular or intradentate injection of colchicine. Brain Res 517:157–167. https://doi.org/10.1016/0006-8993(90)91021-8
37. Evrard PA, Ragusi C, Boschi G et al (1998) Simultaneous microdialysis in brain and blood of the mouse: extracellular and intracellular brain colchicine disposition. Brain Res 786:122–127. https://doi.org/10.1016/s0006-8993(97)01454-6
38. Grundman M, Delaney P (2002) Antioxidant strategies for Alzheimer's disease. Proc Nutr Soc 61:191–202. https://doi.org/. DOI
39. National Research Council (US) Committee (2011) Guide for the Care and Use of Laboratory Animals. Washington (DC)
40. CPCSEA (2003) CPCSEA Guidelines for laboratory animal facility. Indian J Pharmacol 35:257–274

Figures

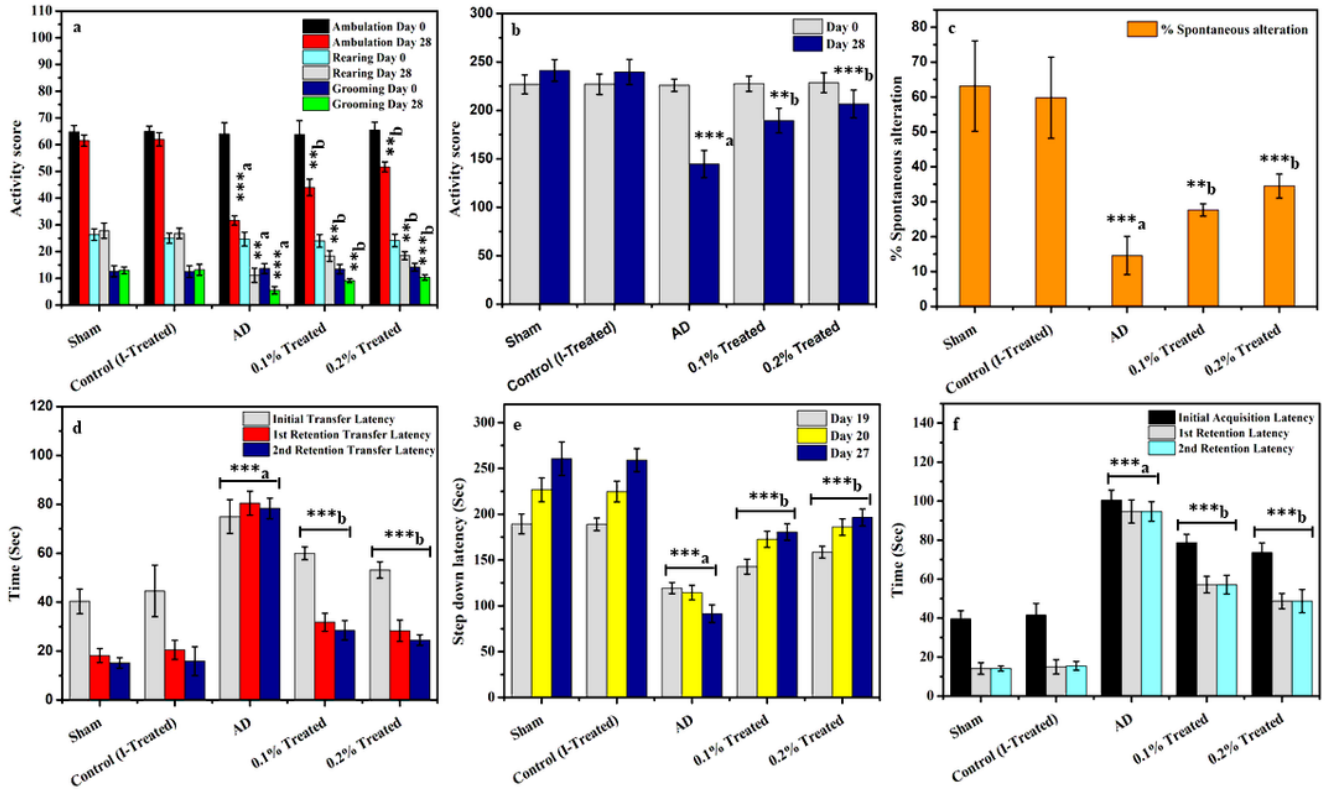

Figure 1

Effect of I on colchicine-induced impairment of memory and learning in Wistar rats evaluated by different behavioral parameters. a: Open-field study, b: Closed-field study, c: Y-Maze test, d: Elevated plus maze test (EPM), e: Step-down latency passive avoidance test, and f: Morris water maze test. Data represented as mean ± SD of six rats in each group. Statistical significance differences were calculated by ANOVA (paired t-test) where 'a' represents Sham vs. AD, 'b' represents AD vs. treated group; significance levels were denoted by * $p<0.05$, ** $p<0.01$, *** $p<0.001$

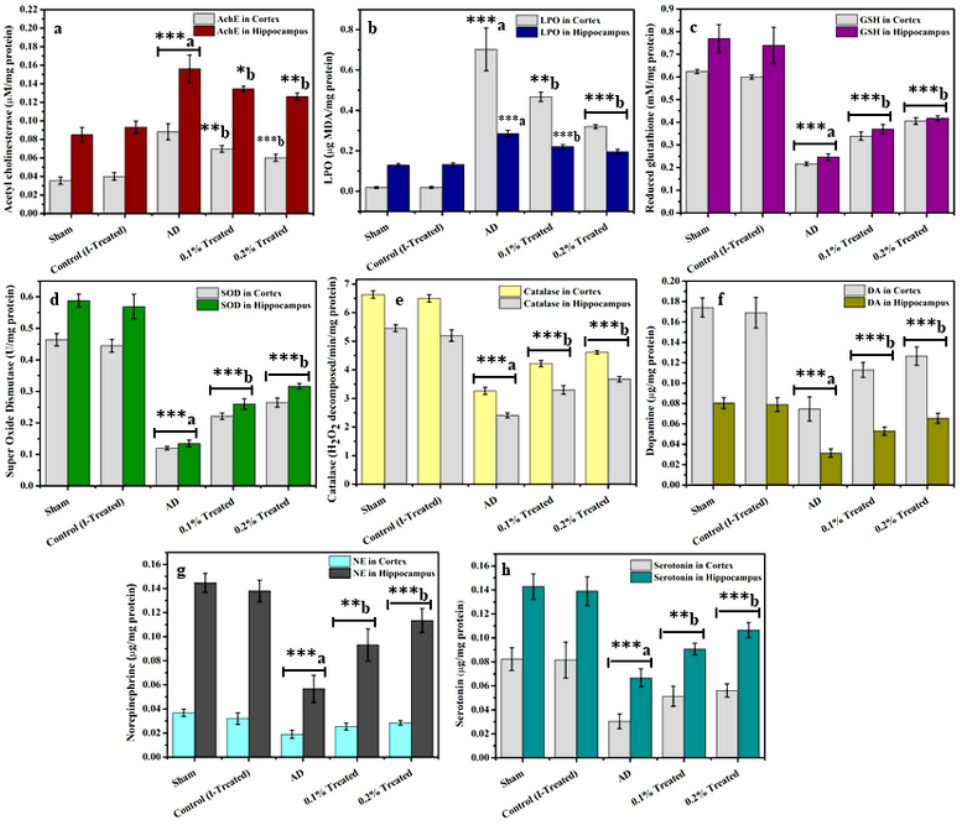

Figure 2

Evaluation of acetylcholinesterase (AchE) enzyme, different oxidative stress markers, and neurotransmitters' profile upon treatment of AD Wistar rats with I. a: AchE level, b: Lipid peroxidation (LPO), c: Reduced glutathione (GSH) level, d: Super oxide dismutase (SOD) level, e: Catalase activity, f: Dopamine (DA), g: Norepinephrine (NE), and h: 5-hydroxytriptamine (5-HT) or Serotonin in cortex and hippocampus of treated and untreated AD Wistar rats along with sham. Data represented as mean ± SD of six rats in each group. Statistical significance differences were calculated by ANOVA (paired t-test) where 'a' represents Sham vs. AD, 'b' represents AD vs. treated group; significance levels were denoted by * $p<0.05$, ** $p<0.01$, *** $p<0.001$

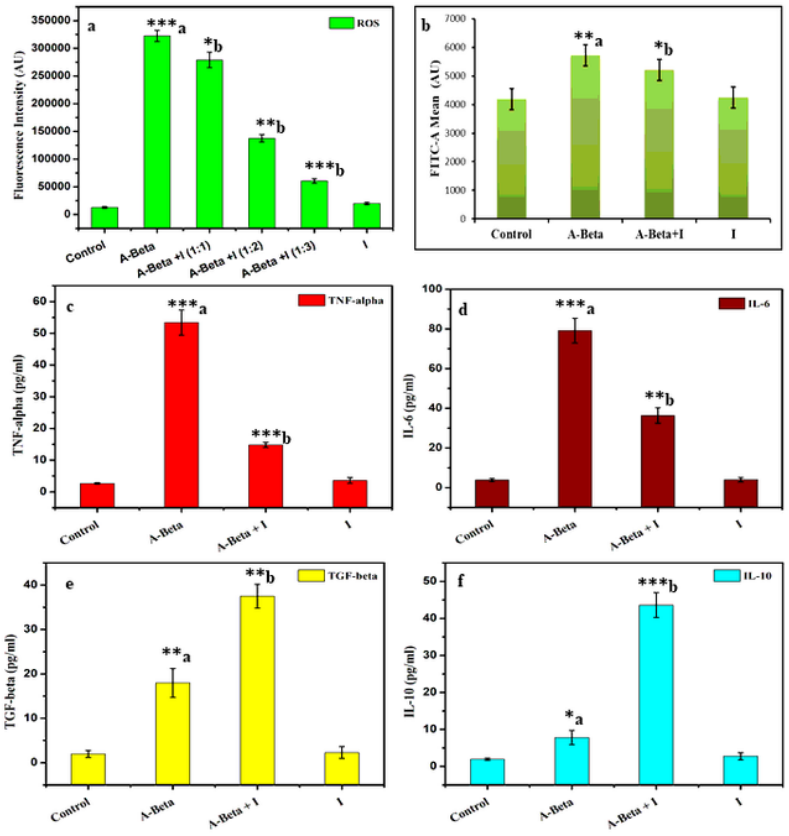

Figure 3

Quantitative measurement of reactive oxygen species (ROS) via a: fluorimeter and b: fluorescence activated cell sorter (FACS) in Aβ_{42}-treated U87 cells and cells treated with I in a dose dependent manner at 1:1- 1:3 molar ratio and at a fixed ratio of 1:1 respectively. Quantitative measurement of pro and anti-inflammatory markers via enzyme linked immunosorbent assay (ELISA) kits. a, b: The levels of pro-inflammatory markers TNF-*α* and IL-6 respectively; c, d: The levels of anti-inflammatory markers TGF-*β* and IL-10 respectively. Significance levels were denoted by * p<0.05, ** p<0.01, *** p<0.001, where 'a' represents control vs. AD, 'b' represents AD vs. treated group

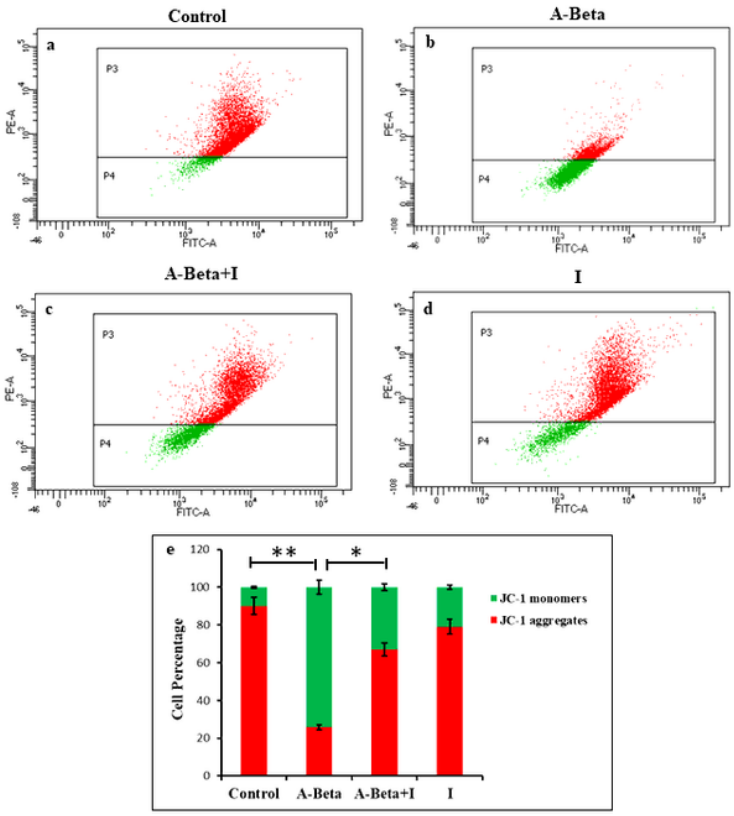

Figure 4

Fluorescence emission spectral shift by JC-1 dye signifying the intact mitochondrial membrane potential in red emission zone and damaged mitochondrial membrane in green emission zone. a: Control U87 cells; b: U87 cells treated with A$\beta_{42;}$ c: Cells treated with Aβ_{42} and I at 1:1 molar ratio; d: U87 cells treated with I; e: Relative cell percentage for control, Aβ_{42}-treated and I-treated cells respectively. Significance levels were denoted by * p<0.05, ** p<0.01

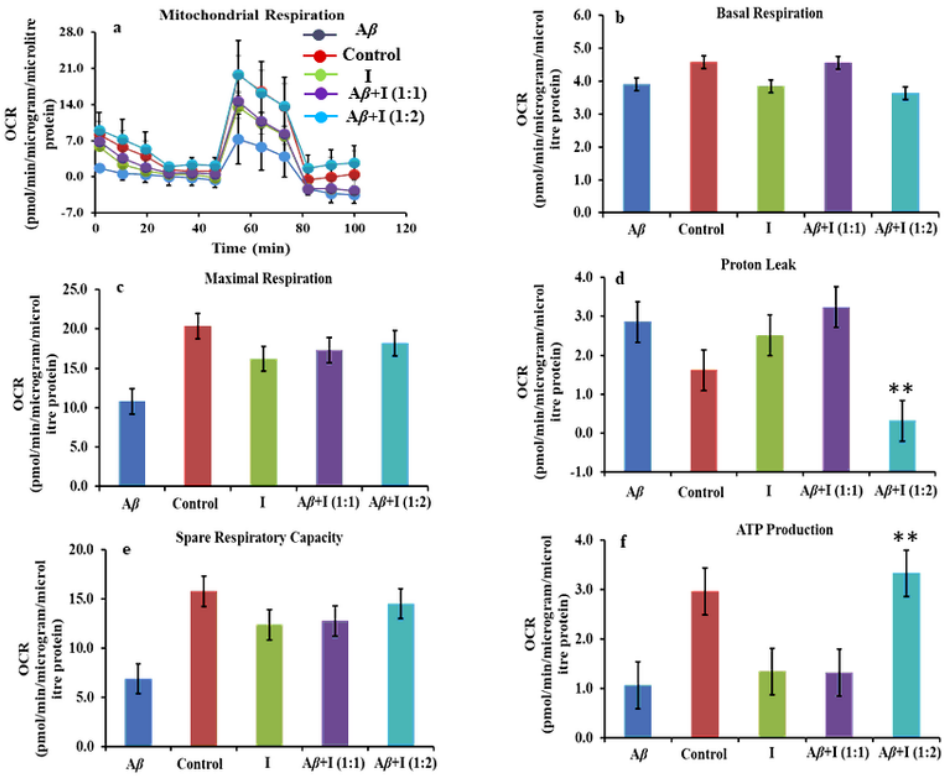

Figure 5

Mitochondrial oxygen consumption rate (OCR) measurement via seahorse experiment. a: Mitochondrial respiration (OXPHOS); b: Basal respiration; c: Maximal respiration; d: Proton leak; e: Spare respiratory capacity; and f: ATP production for Aβ_{42}-treated U87 cells, control cells, I-treated cells at 1:1-1:3 molar ratio and the inhibitor itself respectively. The significance levels were denoted by ** p<0.01

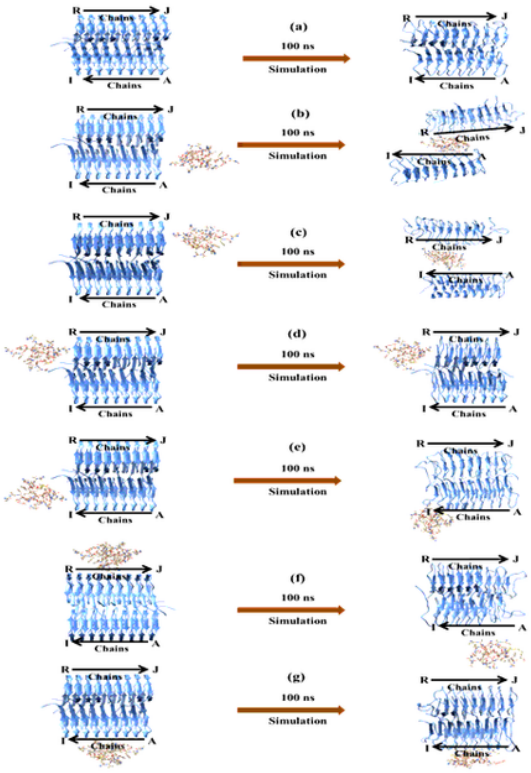

Figure 6

Impact of binding of the PEGylated compound with the fibril structure of Aβ_{42} peptide. Compact structure of the PEGylated compound was placed randomly within interacting distances (<=5 Å) at various faces of the Aβ_{42} fibril structure. For each complex (fibril + molecule) MD simulation run for 100 ns was performed. Panel (a) shows the initial and end structures of the Aβ_{42} fibril without any ligand (PEGylated compound) bound where panels (b-g) show initial and end structures for simulation started with ligand placed near chain A, chain R, chain J, chain I, upper side, lower side, respectively. Aβ_{42} fibril structure (PDB ID: 5KK3) and the ligand (PEGylated compound) are shown in cartoon and stick representations, respectively

Supplementary Files

This is a list of supplementary files associated with this preprint. Click to download.

- TOC.tif
- ManuscriptSI.docx